Microcavities in photonic crystals: Mode symmetry, tunability, and coupling efficiency

Pierre R. Villeneuve, Shanhui Fan, and J. D. Joannopoulos

Department of Physics, Massachusetts Institute of Technology, Cambridge, Massachusetts 02139

(Received 1 March 1996)

We investigate the properties of resonant modes which arise from the introduction of local defects in two-dimensional (2D) and 3D photonic crystals. We show that the properties of these modes can be controlled by simply changing the nature and size of the defects. We compute the frequency, polarization, symmetry, and field distribution of the resonant modes by solving Maxwell's equations in the frequency domain. The dynamic behavior of the modes is determined by using a finite-difference time-domain method which allows us to compute the coupling efficiency and the losses in the microcavity. [S0163-1829(96)05135-1]

I. INTRODUCTION

It is well known that the rate of spontaneous radiative decay of an atom scales with the atom-field coupling and with the density of allowed states at the atomic transition frequency. By changing either the atom-field coupling or the density of states, the rate of spontaneous emission can be significantly affected.

In free space, the density of states scales quadratically with the frequency, and the probability of finding an atom in an excited state simply decays exponentially with time. The introduction of boundaries in the vicinity of the atom has the effect of changing the density of allowed states. For example, in the case of a bounded system with perfectly reflecting walls, the density of states is reduced to a spectrally discrete set of very sharp peaks, each corresponding to a resonant mode of the cavity. If the atomic transition frequency falls between any of these peaks, atomic radiative decay can be essentially suppressed. However, if the transition frequency matches one of the resonances, the density of available modes for radiative decay becomes very large, which in turn enhances the rate of spontaneous emission.

It has been suggested recently that photonic crystals could be used to control the rate of spontaneous emission, since they have the ability of suppressing every mode in the structure for a given range of frequencies.[1,2] These crystals behave essentially like three-dimensional dielectric mirrors, reflecting light along every direction in space. In the case where the radiative transition frequency of an atom falls within the frequency gap of the crystal, spontaneous radiative decay can be suppressed.

If a small defect is introduced in the photonic crystal, a mode (or group of modes) can be created within the structure at a frequency which lies inside the gap.[3–8] The defect behaves like a microcavity surrounded by reflecting walls. If the defect has the proper size to support a state in the band gap, and if the radiative transition frequency of the atom matches that of the defect state, the rate of spontaneous emission will be enhanced.

In this paper, we investigate the properties of these defect states: their frequency, polarization, symmetry, and field distribution, as well as their coupling efficiency to modes outside the crystal. We show that, by choosing a proper defect, we can shape the resonance and tune its frequency to suit most any requirement. We also compute the losses of the cavity and show that the quality factor Q can be made very large by simply increasing the size of the crystal.

II. COMPUTATIONAL METHODS

To investigate the properties of defect states in photonic crystals, two different computational approaches are used. The first solves Maxwell's equations in the frequency domain, while the second solves the equations in the time domain. These two methods reveal different information about the cavity. The frequency-domain method yields the frequency, polarization, symmetry, and field distribution of every eigenmode in the cavity, and the time-domain method allows us to determine the temporal behavior of the modes. By looking at the evolution of the fields in time, we will be able to determine the coupling efficiency, the scattering, and the quality factor of the cavity.

A. Frequency domain

In the first method, the fields are expanded into a set of harmonic modes; the wave equation for the magnetic field is written in the form

$$\nabla \times \left\{ \frac{1}{\epsilon(r)} \nabla \times H(r) \right\} = \frac{\omega^2}{c^2} H(r). \tag{1}$$

Equation (1) is an eigenvalue problem which can be rewritten as

$$\Theta H_n = \lambda_n H_n, \tag{2}$$

where Θ is a Hermitian differential operator and λ_n is the nth eigenvalue, proportional to the squared frequency of the mode. We solve Eq. (2) by using a variational approach, where each eigenvalue is computed separately by minimizing the functional $\langle H_n | \Theta | H_n \rangle$. This method is described in more detail in Refs. 9 and 10. Briefly, to find the minimum, we use the conjugate gradient method with preconditions, keeping H_n orthogonal to the lower states. The conjugate gradient method has the advantage of being more efficient than the traditional method of steepest descents, in that it requires less iterations to reach convergence. In order to minimize the functional, we need to calculate

$$\Theta H_n(r) = \left\{ \nabla \times \frac{1}{\epsilon(r)} \nabla \times \right\} H_n(r). \tag{3}$$

Since the curl is a diagonal operator in reciprocal space, and $1/\epsilon(r)$ is a diagonal operator in real space, each of these operators is computed in the space where it is diagonal by going back and forth between real and reciprocal space using fast Fourier transforms (FFT's). This allows the operator Θ to be diagonalized without storing every element of the $N \times N$ matrix; instead, only the N elements of H_n need be stored. In turn, we will be able to consider structures of very large dimensions.

B. Time domain

The second method solves Maxwell's equations in real space, where the explicit time dependency of the equations is maintained. The equations for the electric and magnetic fields can be written as

$$\frac{\partial}{\partial t} H(r,t) = -\nabla \times E(r,t), \tag{4}$$

$$\epsilon(r) \frac{\partial}{\partial t} E(r,t) = \nabla \times H(r,t). \tag{5}$$

These equations are discretized on a simple cubic lattice,[11] where space-time points are separated by fixed units of time and distance. The derivatives are approximated at each lattice point by a corresponding centered difference, which gives rise to finite-difference equations. By solving these equations, the temporal response of the microcavities can be determined.

In solving Eqs. (4) and (5), special attention must be given to the fields at the boundary of the finite-sized computational cells. Since information outside the cell is not available, the fields at the edges must be updated using boundary conditions. In our simulations, we used Mur's second-order absorbing boundary conditions in order to minimize back reflections into the cell.[12]

III. TWO-DIMENSIONAL CRYSTALS

We begin by investigating the properties of a microcavity in a two-dimensional photonic crystal. The crystal consists of a perfect array of infinitely long dielectric rods located on a square lattice of length a. Each rod has a radius of $0.20a$, and a refractive index of 3.4. By normalizing every parameter with respect to the lattice constant a, we can scale the microcavity to any length scale simply by scaling a.

A. Mode symmetry

We investigate the propagation of electromagnetic fields in the plane normal to the rods. Since the rods have translational symmetry along their axes, the waves can be decoupled into two transversely polarized modes, transverse electric (TE) and transverse magnetic (TM), depending on whether the electric or magnetic field is normal to the rods. The allowed modes in this structure are computed by using the frequency domain approach described in Sec. II A. A large gap for TM modes is found between the frequencies $f = 0.29c/a$ and $f = 0.42c/a$. A similar gap for TE modes does not exist. Since TE and TM modes are linearly inde-
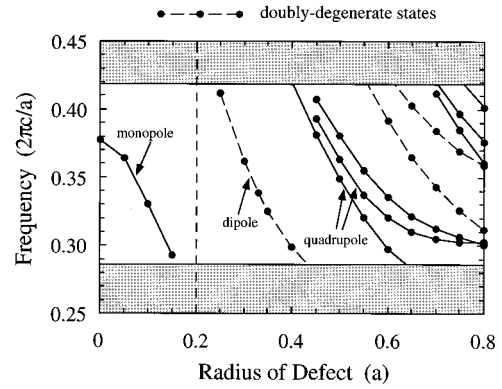

FIG. 1. Frequency of the defect states in an array of dielectric rods with radius $0.20a$. The defect is introduced by changing the radius R of a single rod. The case where $R = 0.20a$ corresponds to a perfect array, while the case where $R = 0$ corresponds to the removal of a rod. The shaded regions indicate the edges of the band gap.

pendent, it is possible to study the behavior of each polarization separately. For the remainder of this section, only TM modes will be considered.

A defect is now introduced into the perfect array of rods. The defect can have any shape or size; it can be made by changing the refractive index of a rod, modifying its radius, or removing a rod altogether. The defect could also be made by changing the index or the radius of several rods. Here we choose to modify the radius of a single rod. The modes in the crystal are computed using a supercell approximation, which consists of placing a large crystal with a defect into a supercell and repeating it periodically in space. In the example below, the supercell contains a 7×7 crystal.

We begin with a perfect crystal—where every rod has a radius of $0.20a$—and gradually reduce the radius of a single rod. Initially, the perturbation is too small to localize a mode in the crystal. When the radius reaches $0.15a$, a resonant mode appears in the vicinity of the defect. Since the defect involves removing dielectric material in the crystal, the mode appears at a frequency close to the lower edge of the band gap. As the radius of the rod is further reduced, the frequency of the resonant mode sweeps upward across the gap, and eventually reaches $f = 0.38c/a$ when the rod is completely removed. Figure 1 shows the frequency of the mode for several values of the radius. The frequency of the mode can be tuned by simply adjusting the size of the rod.

The electric field distribution of the resonant mode is shown in Fig. 2(a) for the specific case where the radius is equal to $0.10a$. The electric field is polarized along the axis of the rods and decays rapidly away from the defect. Since the field does not have a node in the azimuthal direction, it is labeled a monopole. The frequency of the mode is $f = 0.33c/a$.

Instead of reducing the size of a rod, it would also have been possible to increase its size. Again, starting from a perfect crystal, we gradually increase the radius of a rod. When the radius reaches $0.25a$, two doubly degenerate modes appear at the top of the gap. Since the defect involves adding material, the modes sweep downward across the gap as the radius increases. The modes eventually disappear into the continuum below the gap when the radius becomes larger
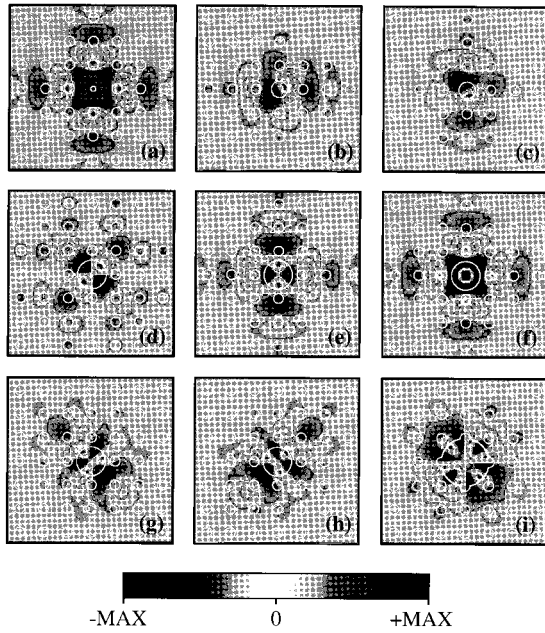
FIG. 2. Electric-field distribution of TM defect states in an array of dielectric rods for various defect sizes. (a) Monopole, $R = 0.10a$. (b) and (c) Doubly degenerate dipoles, $R = 0.33a$. (d) and (e) Nondegenerate quadrupoles, $R = 0.60a$. (f) Second-order monopole, $R = 0.60a$. (g) and (h) Doubly degenerate hexapoles, $R = 0.60a$. (i) Dodecapole, $R = 1.00a$. The white circles indicate the position of the rods.

than $0.40a$ (see Fig. 1). The field distribution of the two doubly degenerate modes is shown in Figs. 2(b) and 2(c) for the case where $R = 0.33a$. The modes are labeled dipoles since they have two nodes in the plane.

By increasing the radius further, a large number of resonant modes can be created in the vicinity of the defect. This is shown again in Fig. 1. Several modes appear at the top of the gap: first a quadrupole, then another (nondegenerate) quadrupole, followed by a second-order monopole and two doubly degenerate hexapoles. These modes also sweep downward across the gap as the defect is increased. The modes are shown in Figs. 2(d)–2(h) for the case where $R = 0.60a$.

Figure 2(i) shows the field distribution for one of the many resonant modes which exist in the cavity when R is equal to the lattice constant a. The defect state resembles a whispering-gallery mode found in a microdisk laser. The field has many nodes (12 in this case) and is located mostly at the edges of the defect.

B. Coupling efficiency

In order to couple energy into the cavity, it is necessary to transfer energy through the walls of the crystal. Incident light can transfer energy to the resonant mode by the evanescent field across the array of rods. To compute the coupling efficiency, we use the time-domain approach described in Sec. II B, and consider a finite-sized 7×11 crystal in which a single rod has been removed. Plane waves are sent at normal incidence, and the transmission is computed through the crystal. The setup is shown in Fig. 3(a).

The incident light must have some component of the same symmetry as that of the cavity mode in order to couple into
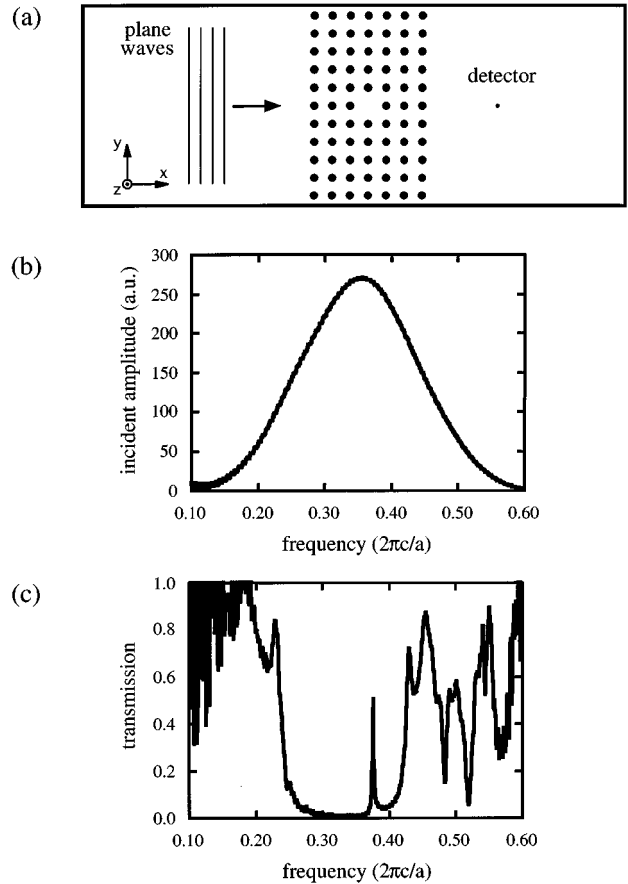

FIG. 3. (a) Setup for the computation of the coupling efficiency. (b) Gaussian frequency profile of the incident pulse. (c) Normalized transmission through the cavity as a function of frequency.

the cavity. In the case of a missing rod, we have shown that the resonant mode has even symmetry with respect to the xz plane passing through the middle of the defect. We have also shown that the resonant mode has even symmetry with respect to the xy plane, since the electric field is polarized along the z direction. Therefore, plane waves should be able to couple energy efficiently into the cavity as long as they are polarized along the z direction.

Instead of studying the steady-state response of plane waves, one frequency at a time, a single pulse of light is sent onto the crystal with a wide frequency profile. The spectrum of the incident pulse is shown in Fig. 3(b). It has a Gaussian profile centered at $f = 0.35c/a$ and a width of $0.20c/a$ which extends beyond the edges of the gap. The electric field is polarized along the axis of the rods. The transmission through the crystal is computed at a single point, marked "detector" in Fig. 3(a). The transmission is normalized with respect to the incident amplitude. Results are shown in Fig. 3(c).

A wide gap can be seen in the transmission spectrum. The gap extends from $f = 0.24c/a$ to $f = 0.42c/a$. Although the upper frequency of the gap matches that of Fig. 1, Fig. 3(c) appears to have a larger gap than Fig. 1. We recall, however, that the gap in Fig. 1 applies to all directions in the plane whereas the one in Fig. 3(c) applies only to propagation along the direction of the incident waves.

The modes inside the gap are strongly attenuated. They cannot propagate through the crystal and are reflected back.

On the other hand, modes outside the gap can be transmitted efficiently; some frequencies have a transmission coefficient close to unity. This suggests that the modes undergo little scattering or reflection as they propagate through the crystal. The rapid fluctuations of the transmission at low frequencies are not real features of the system; they arise from the small signal-to-noise ratio at the edges of the Gaussian frequency profile.

Figure 3(c) also shows the presence of a sharp resonance inside the gap. The coupling efficiency from the incident plane waves to the resonant mode is determined by the height of the peak. Since the resonant mode radiates into a wide range of angles, and since the transmission is computed at a single point in space, only a fraction of the transmitted fields is detected. The coupling efficiency is computed to be slightly larger than 50%.

C. Quality factor

The quality factor Q is a measure of the losses in the cavity. Since the reflectivity of the crystal surrounding the defect increases with the number of rods, we expect that Q will also increase with the size of the crystal. To compute Q, we choose to use an approach which first involves pumping energy into the cavity, then monitoring its decay. We recall that the quality factor is defined as[13]

$$Q = \frac{\omega_0 E}{P} = -\frac{\omega_0 E}{dE/dt}, \qquad (6)$$

where E is the stored energy, ω_0 is the resonant frequency, and $P = -dE/dt$ is the dissipated power. A resonator can therefore sustain Q oscillations before its energy decays by a factor of $e^{-2\pi}$ (or approximately 0.2%) of its original value. After exciting the resonant mode, the total energy can be monitored as a function of time, and Q can be computed from the number or optical cycles required for the energy to decay.

Before presenting the results, we note that the Q factor could also have been computed using a different method. We recall that Q can be defined as $\omega_0/\Delta\omega$, where $\Delta\omega$ is the full width at half-power of the resonator's Lorentzian response. By computing $\Delta\omega$ from transmission calculation, we could have estimated the value of Q. This method, however, would have led to larger uncertainties, especially for large values of Q.

We consider again a finite-sized crystal made of dielectric rods where a single rod has been removed. The crystal dimensions are $N \times N$, where N is an odd number. We compute Q for several values of N.

In order to excite the resonance efficiently, the initial conditions are chosen such that the pump mode and the resonant mode have a large overlap. Since the resonant mode is a monopole, we chose to initialize the system with a Gaussian field profile centered around the defect. The energy inside the cavity was then measured over time. During the initial stages of the decay, every mode—except the high-Q one—quickly radiated away, leaving only the energy associated with the resonant mode inside the cavity. The mode continued its slow exponential decay. From the rate of decay, we computed Q.
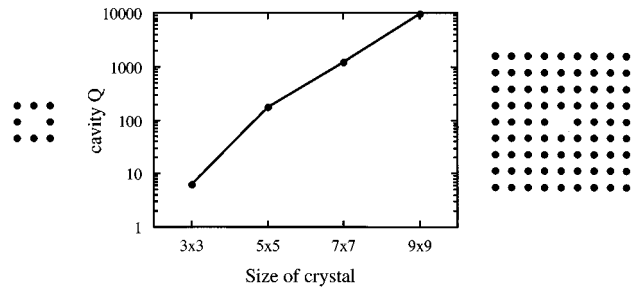

FIG. 4. Quality factor as a function of the size of the crystal.

The value of Q is shown in Fig. 4 as a function of the size of the crystal. Q increases exponentially with the number of rods. It reaches a value close to 10^4 with as little as four lattices on either side of the defect, in agreement with our previous results, which showed strong confinement at the resonance. Since the only energy loss in the structure occurs by tunneling through the edges of the crystal, Q does not saturate even for a very large number of rods.

IV. THREE-DIMENSIONAL CRYSTALS

In order to control every property of a resonant mode, the mode must be completely isolated from the continuum. Three-dimensional photonic crystals have the ability to isolate a mode by opening a complete band gap along every direction in 4π steradians.

A. Crystal geometry

The fabrication of three-dimensional (3D) crystals poses a great challenge. It is equally as important to find a geometry which lends itself to microfabrication as it is to design a structure that generates a large gap. In the past five years, several different geometries have been suggested for the fabrication of 3D crystals.[14–18] Figure 5 shows one such geometry. It is designed to be built layer by layer using two different materials. The materials are chosen such that one may be removed at the end of the fabrication process. The resulting structure is a connected dielectric network filled with air. Since the size of the gap scales with the index contrast between the different materials, the use of air optimizes the size of the gap.
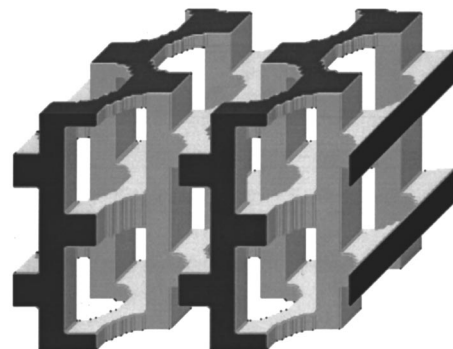

FIG. 5. Three-dimensional photonic crystal. The dielectric material is shown in gray, with edges in black. The rest of the structure is filled with air.
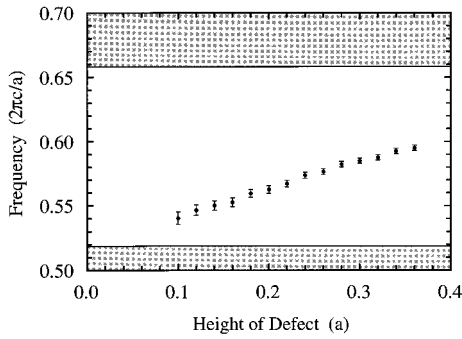
FIG. 6. Frequency of the resonant mode as a function of the defect height in units of lattice constants. The defect is introduced by breaking one of the dielectric ribs. The shaded regions indicate the edges of the band gap.

The structure shown in Fig. 5 could be fabricated, for example, with GaAs and $Al_xGa_{1-x}As$; the connected network could be made of GaAs, while $Al_xGa_{1-x}As$ could be used as a sacrificial material. After selectively removing the $Al_xGa_{1-x}As$, the resulting gap would extend from $f=0.52c/a$ to $f=0.66c/a$, assuming a refractive index of 3.4 for GaAs at 1.55 μm.[19] A more detailed description of the fabrication process of this crystal can be found in Ref. 18.

B. Resonant mode

As we have shown in Sec. III, the introduction of a defect in a 2D crystal can create one or more sharp resonant modes in the vicinity of the defect. The same holds for 3D crystals. In the case of 3D crystals (such as the one shown in Fig. 5), a defect can be made either by adding extra dielectric materials, or by breaking a rib. Either of these defects could be implemented during the growth sequence in one of the layers.

In this section, we choose to break a single dielectric rib at the center of the crystal shown in Fig. 5. The defect is created by cutting across one of the vertical ribs with an air disk. The radius of the disk is $0.27a$, where a is the lattice constant of the crystal. The overall size of the defect is adjusted by varying the height H of the disk. If the size of the defect is properly chosen, a single localized state appears in the gap. Figure 6 shows the frequency of the state as a function of H. Again, the frequency can be tuned by changing the size of the defect. Since the defect consists of removing dielectric material, the resonance appears at the bottom of the gap and moves upward as the size of the defect increases. As we have shown in Fig. 1, the curve which runs through the points need not vary linearly with the size of the defect. Furthermore, the volume of dielectric material removed does not vary linearly with H. When $H=0.16a$, the disk begins to overlap with the horizontal dielectric ribs, and has the effect of removing a larger volume of material per unit length H.

The error bars arise from numerical uncertainty which is due to size limitations in our simulations. The modes are computed in a $2\times2\times2$ supercell with 32 FFT points per unit cell length (or a total of 2.6×10^5 FFT points). To estimate the size of the error bars, the frequency of the resonant mode was computed at both the Γ and X points of the first Brillouin zone in reciprocal space. The X point—which lies in the vertical direction in Fig. 5—was chosen since the mode
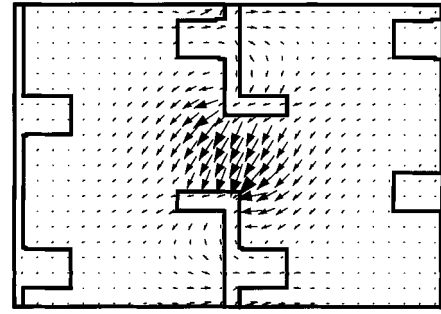

FIG. 7. Vector plot of the electric field in a vertical plane passing through the middle of the defect. The overlay indicates the edges of the crystal. The defect is located at the center of the crystal, and is created by breaking one of the dielectric ribs.

exhibits the largest delocalization along that direction, which should lead to the largest deviation in frequency from the computed value at Γ. As expected, the error bars decrease in size when the resonant mode moves toward the center of the gap since the mode becomes more strongly localized, i.e., the attenuation through each unit cell becomes larger.

A vector plot of the resonant mode is shown in Fig. 7 for the specific case where $H=0.32a$. The electric field is shown in a vertical plane through the middle of the defect. The state is localized in all three dimensions, and the field has even symmetry with respect to the plane. The electric field "jumps" from one edge of the broken rib to the other, while the magnetic field has the shape of a torus and runs around the electric field. The frequency of the mode is $f=0.59c/a$. The symmetry of the mode can be changed by choosing a different type of defect with a different shape or size.

A time-domain analysis reveals the same overall results as those presented in Secs. III B and III C; incident light can transfer energy to the resonant mode by the evanescent field across the crystal, and the quality factor Q increases exponentially with the size of the crystal. We computed the Q factor for the mode shown in Fig. 7 as a function of the size of the crystal, using a similar excitation scheme as the one used in Sec. III C. Results are shown in Fig. 8. The overall cell size is plotted along the x axis. In the case of a crystal with dimensions $2n\times2n\times2n$, the defect is surrounded by n unit cells in every direction. Since the resonant mode is surrounded in three dimensions, the only loss mechanism occurs from coupling to the continuum through the walls of finite thickness.
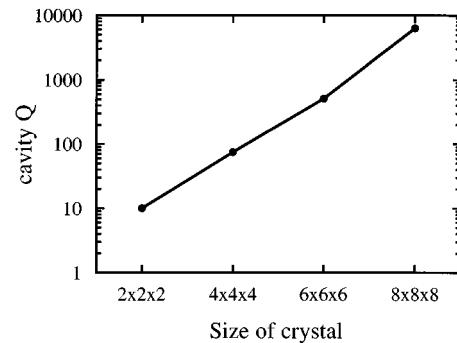

FIG. 8. Quality factor as a function of the size of the three-dimensional crystal.

The growth rate of Q per unit cell is proportional to the localization strength of the resonant mode. For the case shown in Fig. 8, the resonance is located at midgap, a distance $(\omega_{edge}-\omega_0)/\omega_0$ of 12% from the edges of the gap. For purposes of comparison, the resonance in the 2D crystal shown in Fig. 4 was located a distance of 11% from the closest gap edge. Since both resonances are located at almost equal distances from the closest gap edge, the exponential growth of Q is similar in both cases.

V. CONCLUSION

We have shown that photonic crystals can be used for the fabrication of high-Q microcavities. By introducing a defect in a photonic crystal, sharp resonant states can be created in the vicinity of the defect. The properties of these modes—frequency, polarization, symmetry, and field distribution—can be controlled by changing the nature and the size of the defect. Furthermore, the resonant states can couple to external modes by the evanescent field across the crystal, and the quality factor Q increases exponentially with the crystal's size.

[1] E. Yablonovitch, J. Opt. Soc. Am. B **10**, 283 (1993).

[2] P. R. Villeneuve and M. Piché, Prog. Quantum Electron. **18**, 152 (1994).

[3] R. D. Meade, K. D. Brommer, A. M. Rappe, and J. D. Joannopoulos, Phys. Rev. B **44**, 13 772 (1991).

[4] E. Yablonovitch, T. J. Gmitter, R. D. Meade, A. M. Rappe, K. D. Brommer, and J. D. Joannopoulos, Phys. Rev. Lett. **67**, 3380 (1991).

[5] S. L. McCall, P. M. Platzman, R. Dalichaouch, D. Smith, and S. Schultz, Phys. Rev. Lett. **67**, 2017 (1991).

[6] K. M. Leung, J. Opt. Soc. Am. B **10**, 303 (1993).

[7] A. A. Maradudin and A. R. McGurn, in *Photonic Band Gaps and Localization*, edited by C. M. Soukoulis (Plenum, New York, 1993).

[8] K. Busch, C. T. Chan, and C. M. Soukoulis, in *Photonic Band Gap Materials*, edited by C. M. Soukoulis (Kluwer, Dordrecht, 1996).

[9] J. D. Joannopoulos, R. D. Meade, and J. N. Winn, *Photonic Crystals* (Princeton, New York, 1995).

[10] R. D. Meade, A. M. Rappe, K. D. Brommer, and J. D. Joannopoulos, Phys. Rev. B **48**, 8434 (1993).

[11] K. S. Yee, IEEE Trans. Antennas Propag. **AP-14**, 302 (1966).

[12] G. Mur, IEEE Trans. Electromagn. Compat. **EMC-23**, 377 (1981).

[13] A. Yariv, *Optical Electronics* (Saunders, Philadelphia, 1991).

[14] E. Yablonovitch, T. J. Gmitter, and K. M. Leung, Phys. Rev. Lett. **67**, 2295 (1991).

[15] K. M. Ho, C. T. Chan, C. M. Soukoulis, R. Biswas, and M. Sigalas, Solid State Commun. **89**, 413 (1994).

[16] H. S. Sözüer and J. P. Dowling, J. Mod. Opt. **41**, 231 (1994).

[17] G. Feiertag, W. Ehrfeld, H. Freimuth, G. Kiriakidis, H. Lehr, T. Pedersen, M. Schmidt, C. Soukoulis, and R. Weidel, in *Photonic Band Gap Materials* (Ref. 8).

[18] S. Fan. P. R. Villeneuve, R. D. Meade, and J. D. Joannopoulos, Appl. Phys. Lett. **65**, 1466 (1994).

[19] *Handbook of Optical Constants of Solids*, edited by E. D. Palik (Academic, New York, 1985).